International Journal of Mechanical, Industrial and Aerospace Sciences
ISSN: 2517-9950
Vol:10, No:1, 2016

Wall Pressure Fluctuations in Naturally Developing Boundary Layer Flows on Axisymmetric Bodies

Chinsuk Hong

Abstract—This paper investigates the characteristics of wall pressure fluctuations in naturally developing boundary layer flows on axisymmetric bodies experimentally. The axisymmetric body has a modified ellipsoidal blunt nose. Flush-mounted microphones are used to measure the wall pressure fluctuations in the boundary layer flow over the body. The measurements are performed in a low noise wind tunnel. It is found that the correlation between the flow regime and the characteristics of the pressure fluctuations is distinct. The process from small fluctuation in laminar flow to large fluctuation in turbulent flow is investigated. Tollmien-Schlichting wave (T-S wave) is found to generate and develop in transition. Because of the T-S wave, the wall pressure fluctuations in the transition region are higher than those in the turbulent boundary layer.

Keywords—Wall Pressure Fluctuation, Boundary Layer Flow, Transition, Turbulent Flow, Axisymmetric Body, Flow Noise.

I. Introduction

WHEN fluids flow over an axisymmetric body, a boundary layer is formed on the surface of the axisymmetric body due to viscosity. The boundary layer flow develops from laminar near the nose of the axisymmetric body into turbulent flow including distinct transition. The wall pressure fluctuations induced by complicated movement of fluid particles in the boundary layer become excitation sources to the body. This sources hence produce structural vibrations generating noise outside and/or inside the body. This mechanism of noise generation is referred to as *flow noise*.

The process of flow evolution over an axisymmetric body is well-known. Laminar flow is initially formed near the stagnation point on the nose of the axisymmetric body. No pressure fluctuation exists in laminar flow. Transition boundary layer flow is then produced, from which a small pressure fluctuation begins to be produced at the location of the minimum static pressure coefficient. The transition boundary layer flow develops in the direction of adverse pressure gradient, i.e, $\partial P/\partial x > 0$. The small pressure fluctuation in the transition is called as the Tollmien-Schlichting wave(T-S wave). The intensity of the T-S wave increases, resulting in turbulent bursting, as flowing downstream. The flow eventually becomes a fully developed turbulent boundary layer flow. Due to the rapid development of the T-S wave in the transition boundary layer, the pressure fluctuation shows strong nonlinearity [1]. Perraud [2] and Abarbanel [3] showed that the pressure fluctuations in transition boundary layer possibly are 10∼25dB higher than those in the turbulent boundary layer although it takes place locally. In this context, the wall pressure fluctuations in developing boundary layer flows are an interesting topic to investigate.

Chinsuk Hong is with the Department of Mechanical Engineering, University College of Ulsan, Republic of Korea (e-mail: cshong@uc.ac.kr).

The wall pressure fluctuations in fully-developed turbulent boundary layer flows were firstly measured over a flat plate with no pressure gradient by Willmarth [4] in 1956. Since then, many researches on wall pressure fluctuations have been conducted theoretically and experimentally, but the results have been applicable mostly for those over flat plates [5], [6]. Flow over axisymmetric bodies is characterized by the behavior of the pressure gradient along the surface. The pressure gradient is favorable around the nose of the axisymmetric body and then turns into being adverse. The curvatures perpendicular to the direction of the flow complicates the flow. The turbulent bursting in the transition at the nose of axisymmetric body has not been elucidated yet, and there have been very few research on this topic [7]. Several research findings on wall pressure fluctuations over axisymmetric bodies have been presented. Perraud [2] measured the wall pressure fluctuations on a long ellipsoidal nose and showed that the estimated convection velocity in the transition region produced at the nose is about 45% of the upstream velocity. Katz, in 1990, conducted a BVT (Bouyancy-propelled Vehicle Test) to measure wall pressure fluctuation. They showed that the root-mean-square value of the wall pressure fluctuation in the transition is about 18dB higher than that in the fully-developed turbulent flow. However, it is likely that the level of wall pressure fluctuation in the transition is further increased by the variation of the angle of attack of the body when the body is vertically running, as pointed by [8]. He showed that a small variation of the angle of attack of the body causes the separation of the flow and this separation lead to the increase of the level of wall pressure fluctuations. The re-attachment as well as the separation is an essential feature of boundary layer flows at the nose of axisymmetric bodies. Arakeri [9] experimentally showed that the wall pressure fluctuations in the re-attachment region are 10 times higher than those in the fully-developed boundary layer flow.

This paper is concerned with the wall pressure fluctuations of an axisymmetric body over which flow is naturally developed from laminar to turbulent flow with distinct transition boundary layer. The shape of the nose of the body is modified to be ellipsoidal and blunt in the front. The measurement is conducted under the condition of a stable zero angle of attack and the separation-free. The natural characteristics of boundary layer flows are thus investigated using frequency spectra of wall pressure fluctuations at nine positions along the surface. The coherence functions and the

phase of the cross-spectrum between two adjacent positions are examined to characterize the wall pressure fluctuations.

In Section II, the experimental setup such as the test facility, test model and measurement instrumentation is explained. The test results are shown and discussions are presented in Section III in terms of auto-spectra, coherence functions and phase of the 7cross-spectra. Conclusions from this study are given finally given in Section IV.

II. Experimental Setup

A. Test Facility and Test Model

The measurement is conducted in a low noise wind tunnel shown in Fig. 1. The wind tunnel is an open-jet type having the dimension of 400mm $\times$ 400mm. The maximum flow speed is 56 m/s and the turbulent intensity is less than 1% [10]. To reduce the background noise an open-jet is installed in an anechoic chamber. The background noise is further reduced by using a silencer and a noise cancellation technique in the duct. The background noise level achieved is about 60dB ref. 20μPa at the maximum flow speed.

Fig. 2 shows the schematic shape of the model which consists of a blunt nose, a cylindrical shell and a sharp tail. The model is made of aluminum. The dimensions of the model are 2m long, 160mm in diameter and 10mm in thickness. The shape of nose is formed by a flat surface in the front followed by a modified ellipsoid. To install the model in the anechoic chamber a strut whose section is the shape of NACA0018 is used, so that the flow disturbance due to the strut is minimized.

B. Instrumentation

Two kinds of sensors, manometers and microphones, are mounted in the form of an array along the surface of the test model. The manometers are used to measure static pressures on the surface along the body from the stagnation point to cylindrical part, where the diameter almost reaches the maximum. The locations of the sensors are listed in Table I and shown in Fig. 2. The locations are represented in terms of the arc length from the stagnation point. Nine pressure taps ($\#1 \sim \#9$) are installed along the ellipsoidal surface as shown in Fig. 2. Two more pressure taps ('S' and 'F') are also installed on the flat surface at $x = 0$: one at the stagnation point and the other at (x,r)=(0, 50mm). The diameter of the pressure taps is 1 mm. The static pressures are read by using Micromanometer of Furness Co. Ltd. The static pressure distribution represented by the pressure coefficient, C_p, shows the characteristics of the boundary layer flow field.

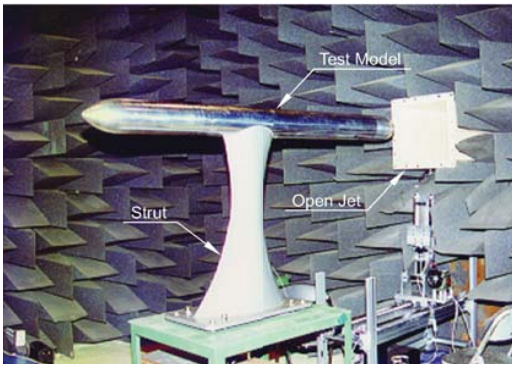

Fig. 1 Axisymmetric body in the anechoic chamber of low noise wind tunnel having 400mm $\times$ 400mm open-jet. The body is supported by a strut having NACA0018 section

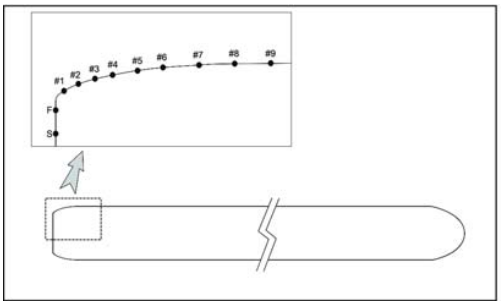

Fig. 2 Shape of the test model and locations of the sensors: S denotes the stagnation point at which a pressure tap is installed and F denotes the front face of the test model at which a pressure tap is also installed. Pressure taps and microphones at #1 to #9 are installed on different models with the same shape and dimensions.

The microphones are also used to measure the wall pressure fluctuation on the surface of the ellipsoidal part of the axisymmetric body. Nine microphones ($\#1 \sim \#9$ in Fig. 2) are flush-mounted at the same locations as the pressure taps on the ellipsoidal surface where the flow is developed from laminar to turbulent with distinct transition region at the flow speeds of interest. Note that no microphones are installed at the location labeled 'S' and 'F' in Fig. 2. Condense type microphones having diaphragm of 1/8 in. diameter, made by Brüel & Kjaer, were used. The measurement is affected by the size of diaphragm of the microphones. Since the size of the diaphragm of the microphones is finite, the signal captured by the diaphragm is spatially averaged over the area of the diaphragm. At low frequencies, the averaged signal can be equivalent to a signal at a point. At higher frequencies, however, the averaged signal decreases with the increase of the frequency [11]. Blake [12] used a pin-hole system to reduce the sensing area. However, the attenuation due to the pin-hole system should be taken into account by the calibration of the pin-hole system. The microphones having the diaphragm of 1/8 in. in diameter are small enough to cover the frequency range of interest in this study. We analyzed the signals taken from the microphones without other calibrations or compensations.

Fig. 3 shows the instrumentation for measuring the wall pressure fluctuations. The signal from the microphone is conditioned using pre-amplifiers and is filtered to remove the low frequency contaminations due to machinery used for tunnel operations. A spectrum analyzer is used to clarify the characteristics of the wall pressure fluctuations. The analyzed data are shared with a personal computer for further data processing.

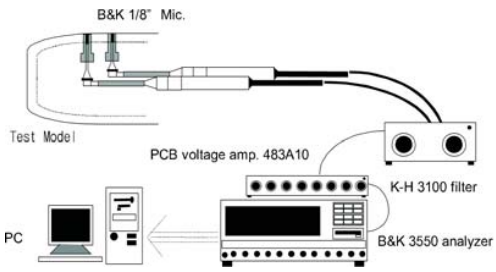

Fig. 3 Schematic diagram of the measurement system of wall pressure fluctuations

TABLE I
SENSOR POSITIONS MEASURED WITH THE ARC-LENGTH ALONG THE SURFACE WITH RESPECT TO THE STAGNATION POINT

Sensor N^o	s(mm)	Remarks
S	0	Pressure Tap only
F	50	Pressure Tap only
#1	80	
#2	90	
#3	103	
#4	116	
#5	133	
#6	150	
#7	175	
#8	199	
#9	223	

III. RESULTS AND DISCUSSION

A. Static Pressures and Flow Regime

The static pressures at the specified locations are measured at the free stream velocities of 10, 20 30, 40, and 50 m/s and the static pressure coefficients are then calculated as

$$C_p = \frac{P - P_\infty}{\frac{1}{2}\rho U_\infty^2}, \quad (1)$$

where P is the measured static pressure, P_∞ is the reference pressure, ρ is the density of air and U_∞ is the upstream velocity.

Fig. 4 shows the variation of the static pressure coefficients with locations along the body surface. The pressure coefficient decreases downstream as the arc length increases from the pressure tap 'S' to #1, showing the favorable pressure gradient. This favorable pressure gradient changes into adverse pressure gradient at the static pressure tap #1. This means that the fluid particle accelerates around this point. It is noted that the variation of the pressure coefficient is independent on the upstream velocity.

B. Background Noise Levels

Before measuring the wall pressure fluctuation using the flush-mounted microphones, we measured the background noise without the body in the test section at flow speeds of 10, 20, 30, 40, and 50 m/s. The microphone to measure the background noise is located at a point 1100mm apart

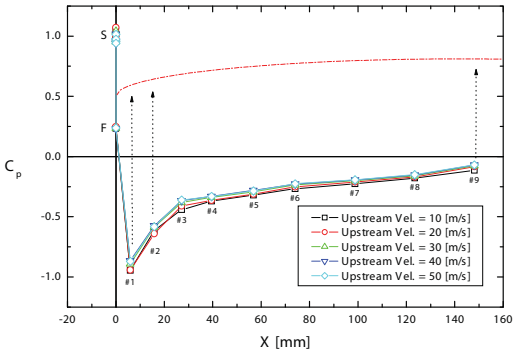

Fig. 4 Variation of static pressure coefficients with upstream velocities of 10, 20, 30, 40 and 50 m/s. 'S' denotes the stagnation point and 'F' denotes the front face. The dot-dashed line shows the shape of the axisymmetric body

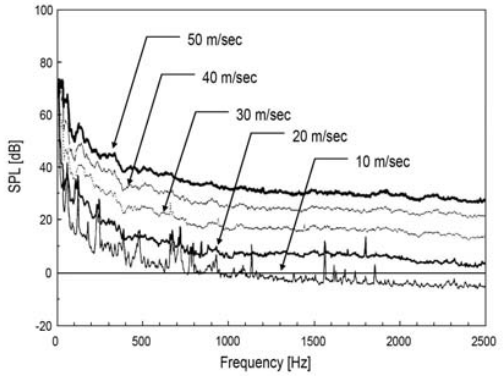

Fig. 5 Background noise levels for open-jet speeds of 10, 20, 30, 40 and 50 m/s

perpendicularly from the center of the flow from the open-jet. This configuration prevents the microphone from contamination by the pressure fluctuation of the in-flow. Fig. 5 shows the measured background noise levels at each flow speed. It can be seen that the background noise level is about 40dB at high frequencies above 1kHz and less than 30dB at the frequencies between 200Hz and 1kHz when the flow speed is 50 m/s. The measurement of wall pressure fluctuations is restricted by the level of background noise. We improved the test condition of background noise using an anechoic chamber and a silencer and an active control technique in the duct leading to the open-jet, as described above.

C. Wall Pressure Fluctuations

The wall pressure fluctuations are analyzed for the upstream velocities of 30 m/s and 40 m/s at locations where the boundary layer flow is naturally developed from laminar to turbulent with a distinct transition region in the range of microphone locations. The upstream velocities correspond to Reynolds numbers of $\mathrm{Re}_D = 3.20 \times 10^5$ and $\mathrm{Re}_D = 4.27 \times 10^5$, respectively, with respect to the maximum diameter of the body. Fig. 6 shows the spectra of the wall pressure fluctuations at the microphone locations $\#1 \sim \#5$ for $\mathrm{Re}_D = 3.20 \times 10^5$. Apart from the contamination due to the background noise below 200Hz, the wall pressure fluctuations at #1 and #2 are

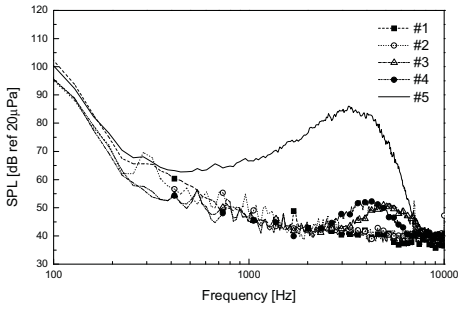

Fig. 6 Spectra of wall pressure fluctuations at microphones $\#1 \sim \#5$ when $\mathrm{Re}_D = 3.20 \times 10^5$

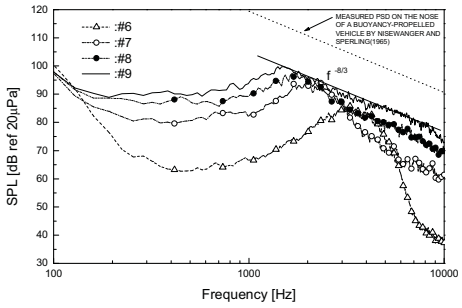

Fig. 7 Spectra of wall pressure fluctuations at microphones $\#6 \sim \#9$ when $\mathrm{Re}_D = 3.20 \times 10^5$. The straight solid line represents the slope of the spectrum at high frequencies, while the dotted line represents the slope taken from the result of [13]

relatively lower than others showing a flat spectrum without any particulars. The wall pressure fluctuation at #3 shows a wide maximum centered at about 5kHz and this center frequency is decreased at downstream(#4 and #5). Therefore, when $\mathrm{Re}_D = 3.20 \times 10^5$, the flow is laminar at #1 and #2 followed by the beginning of transition around #3. This feature of the spectra for the microphones at $\#3 \sim \#5$ are caused by the T-S wave.

Fig. 7 shows the spectra of the wall pressure fluctuations at microphone locations $\#6 \sim \#9$ for $\mathrm{Re}_D = 3.20 \times 10^5$. It can be seen that the bandwidth of the wide maximum of the spectrum due to the T-S wave is broadened. The spectrum above 2kHz shows the slope of -8/3 in the log-log scale. This slope is the same as the result of [13], which is represented by a dotted straight line in Fig. 7. It should be noted that he performed BVT (Buoyantly-propelled Vehicle Test) in water with a very different Reynolds number of $\mathrm{Re}_D = 6.79 \times 10^6$. Georage [14] showed that the pressure fluctuation due to the interaction of turbulences has the slope of -7/3 using their numerical model obtained from the Fourier transform of the Poisson equation. Hence, the high frequency component of turbulence becomes continually stronger in the downstream of #6 and the flow regime of this region is in the late transition. The level of the wall pressure fluctuation in the late transition reaches about 100dB at #9.

The wall pressure fluctuations at the same locations as above

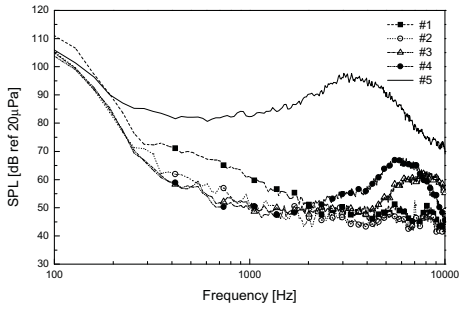

Fig. 8 Spectra of wall pressure fluctuations at microphones $\#1 \sim \#5$ when $\mathrm{Re}_D = 4.27 \times 10^5$

are measured at a higher upstream velocity corresponding to $\mathrm{Re}_D = 4.27 \times 10^5$. Fig. 8 shows the spectra of the wall pressure fluctuations at $\#1 \sim \#5$. It is similar to the case of $\mathrm{Re}_D = 3.20 \times 10^5$ in that the wide maximums of the spectra appear and the levels of the fluctuations increase downstream. However, the center frequency of the wide maximum is decreased downstream, due to the increased boundary layer thickness. In the same context, the center frequency of the wide maximum is decreased as the upstream velocity is increased. Fig. 9 shows the spectra of wall pressure fluctuations at $\#6 \sim \#9$. The spectra show the general feature of fully developed turbulent boundary layer flows. This feature can be generalized by non-dimensionalization with the so-called inner variable, outer variable or mixed variable. Fig. 10 shows the non-dimensionalized spectra of the wall pressure fluctuations of #6 and further downstream to #9 using the outer variables such as the displacement thickness of the boundary layer (δ^*) and the upstream velocity (U_∞). This result was compared with the experimental result for a flat plate by [15]. For $\omega\delta^*/U_\infty < 1$, the two results well agreed because the wall pressure fluctuations in the boundary layer flow are not affected by the curvature perpendicular to the free stream when the boundary layer thickness is much smaller than the diameter of the axisymmetric body. For higher frequencies such that $\omega\delta^*/U_\infty > 1$, however, the results are much different. Part of the difference is caused by the curvature effect at high frequencies. Spatial averaging effect of microphone diaphragms at high frequencies can cause the monotonic decrease of the spectrum with frequency.

It is interesting that the levels of the wall pressure fluctuations in late transition are higher than those in the fully-developed turbulent boundary layer. For example, in Fig. 7, the wall pressure fluctuations at #7 and further downstream at $\mathrm{Re}_D = 3.20 \times 10^5$, where the flow is considered as a late transition flow, are stronger than those at $\mathrm{Re}_D = 4.27 \times 10^5$ where the flow is a fully-developed turbulent boundary layer flow. It can be also seen that for the same Reynolds number of $\mathrm{Re}_D = 4.27 \times 10^5$, the wall pressure fluctuations being in the late transition flow, shown with solid line in Fig. 8 are about 10dB stronger than those further downstream in the fully-developed turbulent boundary layer flow.

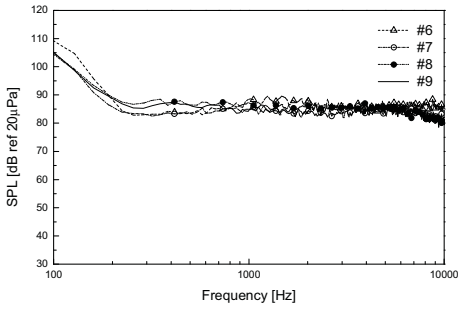

Fig. 9 Spectra of wall pressure fluctuations at microphones $\#6 \sim \#9$ when $\mathrm{Re}_D = 4.27 \times 10^5$

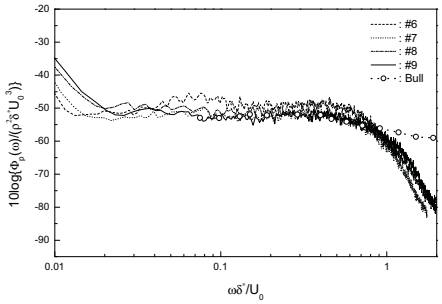

Fig. 10 Non-dimensionalized wall pressure fluctuations at microphones $\#6 \sim \#9$ when $\mathrm{Re}_D = 4.27 \times 10^5$ scaled on outer variables, compared with the result by Bull [15].

D. Interaction of T-S Waves

The interaction of T-S waves can be evaluated from the behavior of the coherence function between two signals from adjacent microphones. The coherence function, $\gamma_{ab}(\omega)$, can be calculated as

$$\gamma_{ab}^2(\omega) = \frac{|\phi_{ab}(\omega)|}{\phi_a(\omega) \cdot \phi_b(\omega)}, \tag{2}$$

where $\phi_a(\omega)$ and $\phi_b(\omega)$ are the auto-power spectra of wall pressure fluctuations at microphone locations a and b, respectively, and $\phi_{ab}(\omega)$ is the cross-power spectrum between the two microphones located at a and b.

Figs. 11 and 12 show the coherence functions between the microphones located at #6 and #7 for $\mathrm{Re}_D = 3.20 \times 10^5$ and $\mathrm{Re}_D = 4.27 \times 10^5$, respectively. Fig. 11 shows a high coherence of about 60% in the frequencies between 2kHz and 4kHz when $\mathrm{Re}_D = 3.20 \times 10^5$. This means that the flow at #6 (upstream) significantly affects the flow at #7 (downstream). It is noted that the frequency range showing high coherence is the same as that showing a wide maximum. It can be thus considered that the high coherence is caused by the interaction of T-S waves in the transition region in this frequency range. On the other hand, the coherence function for $\mathrm{Re}_D = 4.27 \times 10^5$ does not show such a high coherence, as shown in Fig. 12. This is because the microphones in this case are located in the fully-developed turbulent flow where

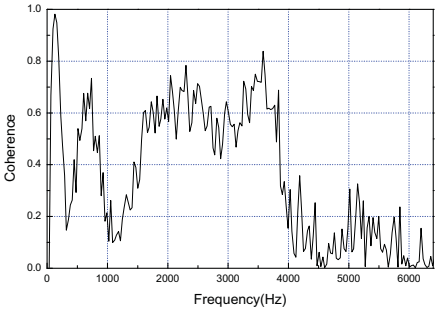

Fig. 11 Coherence function between microphones #6 and #7 when $\mathrm{Re}_D = 3.20 \times 10^5$

the correlation length is very small compared to the distance between the two microphones and the flow can be considered to be spatially random.

E. Convection Velocity

From further investigation on the behavior of the signals from adjacent microphones in terms of the phase of the cross-spectrum, the convection velocity can be estimated. It is known [16] that the convection velocity in the boundary layer can be estimated by using the phase of the cross spectrum as

$$U_c(\omega) = \frac{2\pi\Delta}{\mathrm{d}\theta(\omega)/\mathrm{d}\omega}, \tag{3}$$

where Δ is the distance between the two microphones and $\theta(\omega)$ is the phase at frequency ω. The denominator, $\mathrm{d}\theta(\omega)/\mathrm{d}\omega$, in (3), represents the slope of the phase of the cross spectrum.

Fig. 13 shows the phase of the cross-spectrum between the signals from the microphones #6 and #7. In the frequency range where the signals are strongly correlated, $2 \sim 4$kHz in this case, the phase of the cross spectrum shows a linear dependence of frequency. It can be seen that the phase of the cross spectrum has a distinct slope at frequencies between 1kHz and 5kHz. The convection velocities non-dimensionalized with the upstream velocity are calculated. For each distinct slope, the non-dimensional convection velocities are 0.5, 0.57, 0.65 and 0.85. They increase with frequency. They are comparable to 0.45 for wall pressure fluctuations in the initial transition flow, 0.9 for turbulent spots and 0.7 for fully-developed turbulent boundary layer flows. It can be also concluded from this investigation that microphone locations #6 and #7 are in the late transition region and T-S wave significantly affects the wall pressure fluctuation in the late transition region.

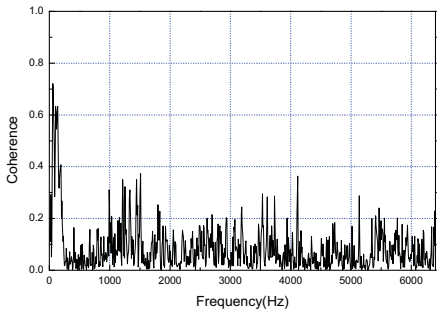

Fig. 12 Coherence function between microphones #6 and #7 when $\mathrm{Re}_D = 4.27 \times 10^5$

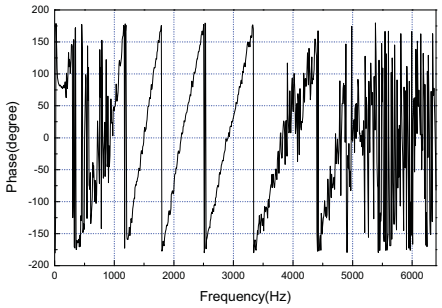

Fig. 13 Phase of the cross-spectrum between microphones #6 and #7 when $\mathrm{Re}_D = 3.20 \times 10^5$

IV. Conclusion

This paper investigated wall pressure fluctuations in boundary layer flows naturally developed from laminar to turbulent with distinct transition region. The wall pressure fluctuations were measured on the curved surface of an axisymmetric body in a low noise wind tunnel using flush mounted microphones. The wall pressure fluctuations in transition flows gave a wide maximum in the spectrum centered at the T-S wave frequency. The level of the fluctuation was increased and the center frequency was decreased, as the upstream velocity was increased. The maximum level of the fluctuations in late transition region was about 10dB higher than that in the fully-developed turbulent boundary layer flow. The convection velocity was in the range of $50\% \sim 85\%$ of the upstream velocities.

References

[1] R. A. Katz, T. A. Galib, J. M. Cembrola, Classical and nonlinear analysis of transitional and turbulent boundary layer flow, in: Proceeding of 2nd Int. Symp. on Perf Enhancement for Marine App., 1990, pp. 119–127.
[2] J. C. Perraud, Studies of laminar-turbulent in air and water wall pressure fluctuations and acoustic emission from the turbulent intermittency, NCA 5 (1989) 17–24.
[3] H. D. Abarbanel, R. A. Katz, T. W. Frison, Nonlinear analysis of high-reynolds-number over a buoyantaxisymmetric body, Physics Review 49 (5) (1994) 4003–4018.
[4] W. W. Willmarth, Wall pressure fluctuations in a turbulent boundary layer, Journal of Acoustical Society of America 28 (1956) 1048–1053.
[5] W. K. Blake, Mechanics of flow-induced sound and vibration(I), Academic Press, Inc., 1986.
[6] W. K. Blake, Mechanics of flow-induced sound and vibration(II), Academic Press, Inc, 1986.
[7] G. C. Lauchle, Hydroacoustics of transitional boundary layer flow, ASME Applied Mechanics Review 44 (12) (1991) 517–531.
[8] M. Gal-el Hak, Unsteay separation on lifting surfaces, Applied Mechanics Review 40 (1987) 441.
[9] V. H. Arakeri, A note on the transition observations on an axisymmetrc body and some related fluctuating wall pressure measurement, Trans. ASME Journal of Fluids Engineering 97 (1975) 82.
[10] J. S. Kim, Measurement of flow noise on an axisymmetric body using a low noise wind tunnel, Tech. rep., Agency for Defense Development (1998).
[11] R. M. Lueptow, Wall pressure transducer spatial resolution, NCA 15/FEDVol 168 (1993) 49–55.
[12] W. K. Blake, Turbulent boundary-layer wall-pressure fluctuations on smooth and rough walls, Journal of Fluid Mechanics 44 (1970) 637–660.
[13] C. R. Nisewanger, F. B. Sperling, Flow noise inside boundary layers of buoyancy-propelled test vehicles, Tech. Rep. 8519, NAVWEPS (1965).
[14] W. K. Georage, P. D. Beuther, R. G. Arndt, Pressure spectra in turbulent free shear flows, Journal of Fluid Mechanics 148 (1984) 155–191.
[15] M. K. Bull, S. W. Thomas, High frequency wall pressure fluctuations in turbulent boundary layers, Physics of Fluids 19 (4) (1976) 597–599.
[16] J. S. Bendat, A. G. Piersol, Engineering Applications of Correlation and Spectral Analysis, Jon Wiley & Sons, Inc., 1993.